

# 'Generalized Permittivity' and Source Sensitivity of Piezoelectric Ceramic Disks

Ørnulf Svan Amundsen<sup>a,\*</sup>, Magne Aanes<sup>a,c</sup>, Jan Kocbach<sup>b,c</sup>, and Magne Vestrheim<sup>a,c</sup>

<sup>a</sup>University of Bergen, Department of Physics and Technology, Postboks 7803, N-5020 BERGEN, Norway

<sup>b</sup>Christian Michelsen Research AS (CMR), P.O. Box 6031 Postterminalen, N-5892 BERGEN, Norway

<sup>c</sup>The Michelsen Centre for Industrial Measurement Science and Technology

## Abstract

Finite element simulations and a reformulation of the electrical admittance for a piezoelectric disk as a 'generalized permittivity' is used to study methods for determine the free, the planar and the clamped permittivity constants. In addition, a method is studied to determine a stiffness constant and a piezoelectric constant. The methods are used to obtain measured values for the material constants considered, and a resulting modified data set is used in FE simulations of the source sensitivity. Further work is needed to demonstrate the soundness and accuracies of the methods and to develop sound methods for the remaining constants.

## 1. Introduction

Finite Element Modeling (FEM) is used extensively in piezoelectric transducer design today, and in applications of such transducers. Accurate values of material constants for piezoelectric and other materials in a transducer construction, can be used in a FEM model together with dimensions to calculate accurately the acoustic field properties. However, there is a need of better methods for material constants determination, and several groups are currently working on this [1–3]. FEM is seen as an important tool in developing more accurate methods for measuring material constants than described in [4]

A 'generalized permittivity' method was used in [3] to study properties of piezoelectric disks including material constants. This method will be discussed further in the present paper, in order to investigate methods for determining the free, the planar and the clamped permittivity constants.

Precise determination of material constants is required for precise simulated acoustical properties such as the source sensitivity. Examples of the influence of material constants on the source sensitivity of a piezoelectric disk are given for two different sets of material data.

## 2. Theory

### 2.1. Material constants

Constitutive equations describing linear properties of piezoelectric materials can be written in the usual four sets of equations using compressed notation [4],

$$T_p = c_{pq}^E S_q - e_{jp} E_j \quad D_i = e_{iq} S_q + \epsilon_{ij}^S E_j, \quad (1)$$

$$T_p = c_{pq}^D S_q - h_{jp} D_j \quad E_i = -h_{iq} S_q + \beta_{ij}^S D_j, \quad (2)$$

---

\*Corresponding author

Email address: [Ørnulf.Amundsen@student.uib.no](mailto:Ørnulf.Amundsen@student.uib.no) (Ørnulf Svan Amundsen)

$$S_p = s_{pq}^E T_q + d_{jp} E_j \quad D_i = d_{iq} T_q + \epsilon_{ij}^T E_j, \quad (3)$$

$$S_p = s_{pq}^D T_q + g_{jp} D_j \quad E_i = -g_{iq} T_q + \beta_{ij}^T D_j, \quad (4)$$

with  $i, j = 1, 2, 3$  and  $p, q = 1, 2, \dots, 6$ .  $T_p$  are the mechanical stress components,  $S_p$  is the mechanical strain components,  $E_i$  are the electrical field vector components and  $D_i$  are the electrical displacement vector components.  $c_{pq}^E$  and  $c_{pq}^D$  are mechanical stiffness constants for constant electric field and constant electric displacement, respectively.  $e_{ip}$ ,  $d_{ip}$ ,  $h_{ip}$  and  $g_{ip}$  are piezoelectric constants,  $\epsilon^S$  are permittivity at constant strain, and  $\epsilon^T$  is the permittivity at constant stress. Each set of equations is expressed by a complete set of material constants. Through matrix calculations, one complete set of constants can be calculated from another [4, 5].

The well known permittivity constants for a piezoelectric ceramic disk and some relations between them can be written as [4-6],

$$\epsilon_{33}^T = \frac{\epsilon_{33}^P}{1 - k_p^2}, \quad (5)$$

$$\epsilon_{33}^P = \frac{\epsilon_{33}^S}{1 - k_t^2}, \quad (6)$$

$$\epsilon_{33}^S = \epsilon_{33}^T (1 - k_p^2) (1 - k_t^2), \quad (7)$$

where  $\epsilon_{33}^P$  is the planar permittivity constant.  $k_p$  and  $k_t$  are the planar and the thickness-extensional coupling factors, respectively, and are given as [4],

$$k_p^2 = \frac{2(k^p)^2}{1 + \sigma^p - 2(k^p)^2}, \quad k_t^2 = k_t = \sqrt{\frac{e_{33}^2}{c_{33}^D \epsilon_{33}^S}}. \quad (8)$$

where,

$$c_{33}^D = c_{33}^E + \frac{e_{33}^2}{\epsilon_{33}^S}, \quad (9)$$

is expressed by constants involved in the first set of constitutive equations, Eq. (1).  $k^p$  and  $\sigma^p$  are the radial piezoelectric coupling factor and the planar Poisson's ratio, respectively [4],

$$k^p = \sqrt{\frac{(e_{31}^p)^2}{c_{11}^p \epsilon_{33}^p}}, \quad \sigma^p = -\frac{s_{12}^E}{s_{11}^E}. \quad (10)$$

The permittivity constants in Eqs. (5)-(7) can be combined with Eqs. (8) and (9) thereby the following two constants used in the constitutive set of equations in Eq. (1) can be expressed by [6],

$$c_{33}^E = c_{33}^D \frac{\epsilon_{33}^S}{\epsilon_{33}^P}, \quad e_{33} = \sqrt{c_{33}^E (\epsilon_{33}^P - \epsilon_{33}^S)}. \quad (11)$$

One usual way to include loss in the description, is to include an imaginary part of the various constants [7, 8]

$$\hat{c}_{pq}^E = c_{pq}^{E'} + i c_{pq}^{E''} = c_{pq}^{E'} (1 + i/Q_{pq}^E), \quad (12)$$

$$\hat{e}_{ip} = e_{ip}' - i e_{ip}'' = e_{ip}' (1 - i/Q_{ip}^e), \quad (13)$$

$$\hat{\epsilon}_{ij}^S = \epsilon_{ij}^{S'} - i \epsilon_{ij}^{S''} = \epsilon_{ij}^{S'} (1 - i/Q_{ij}^S), \quad (14)$$

with  $i, j = 1, 2, 3$  and  $p, q = 1, 2, \dots, 6$ .  $\hat{\cdot}$  denotes complex constants and will be used hereafter.  $'$  and  $''$  denotes the real and the imaginary part of the complex constant, respectively. The dissipation factor is defined as [7, 8]:

$$\tan \delta_{pq}^E = c_{pq}^{E''} / c_{pq}^{E'}, \quad (15)$$

$$\tan \delta_{ip}^e = e_{ip}'' / e_{ip}', \quad (16)$$

$$\tan \delta_{ij}^S = \epsilon_{ij}^{S''} / \epsilon_{ij}^{S'}. \quad (17)$$

## 2.2. Models for piezoelectric vibrations

Simplified models based on different assumptions are interesting when studying the behavior of a piezoelectric transducer. Two simplified models for piezoelectric resonances are of interest in the present work, the radial modes model and the thickness-extensional modes model. However, most of the simulations are made using an axis-symmetric finite element model.

### 2.2.1. Radial modes model

The electrical admittance of the radial modes model is given as [4, 9]

$$Y(f) = \frac{-i\omega\hat{\epsilon}_{33}^p A}{T} \left[ \frac{2(k_p)^2}{1 - \sigma^p - \Im(\eta)} - 1 \right], \quad (18)$$

where  $T$  is the thickness of the disk,  $A = \pi a^2$  is the surface area of the disk and  $a$  is the radius,  $\omega$  is the angular frequency,  $\Im(\eta) = \frac{\eta J_0(\eta)}{J_1(\eta)}$  is Ono's function where  $\eta = \frac{\omega a}{v^p}$ , and  $v^p$  is the velocity in the radial direction,  $J_0$  and  $J_1$  are Bessel functions of first kind and order 0 and 1, respectively. For the radial modes model two limiting values for the electrical admittance can be found

$$\lim_{f \rightarrow 0} \left( Y \frac{T}{i\omega A \epsilon_0} \right) = \hat{\epsilon}_{33r}^T \quad \text{and} \quad \lim_{f \rightarrow \infty} \left( Y \frac{T}{i\omega A \epsilon_0} \right) = \hat{\epsilon}_{33r}^p.$$

$\epsilon_0$  is the permittivity of free space, and the subscript  $r$  denotes relative permittivities.

### 2.2.2. Thickness-extensional modes model (Mason TE model)

In the thickness-extensional (TE) modes model the electrical impedance is given as [4]

$$Z = \frac{1}{Y} = \frac{1}{i\omega C_0} \left( 1 - k_t^2 \tan\left(\frac{1}{2}kT\right) \right), \quad (19)$$

where  $k = \frac{\omega}{c}$ ,  $c = \sqrt{\frac{c_{33}^D}{\rho}}$ , and  $C_0 = \frac{\epsilon_{33}^S A}{T}$  is the clamped capacitance of the disk. The antiresonance frequencies of a lossless element is defined in [4] as the frequencies at maximum impedance ( $Z = i\infty$ ). For the impedance in Eq.(19), this happens when  $\tan(\frac{1}{2}kT) \rightarrow \infty$ , and is true for

$$f_{2,n} = (2n - 1) \frac{c}{2T}, \quad (20)$$

where  $n = 1, 2, 3, \dots$  and subscript  $2$  on the frequency denotes antiresonance. When  $\tan(\frac{1}{2}kT) = 0$  the admittance according to Eq.(19) becomes  $Y = i\omega C_0 = i\omega \frac{\epsilon_{33}^S A}{T}$ . This is fulfilled when

$$f_j = j \frac{c}{T}, \quad (21)$$

where  $j = 1, 2, 3, \dots$ . From this it is clear that the frequencies,  $f_j$ , where  $C_0$  can be found, is midway between two antiresonances, expressed mathematically,  $f_j = \frac{f_{2,n} + f_{2,n+1}}{2}$ ,  $j = n = 1, 2, 3, \dots$

When material losses are used in the description, the IEEE Standard on piezoelectricity, [4], recommends that the parallel resonance frequencies,  $f_p$ , defined by the frequencies at maximum resistance, are used for the antiresonance frequencies defined in Eq. (20). As indicated in [10], the midpoint frequencies,  $f_j$ , where  $C_0$ , and thus also  $\hat{\epsilon}_{33r}^S$  are found is between two parallel resonance frequencies when loss is included in the description. This may provide a method to determine both  $\epsilon_{33r}^{S'}$  and  $\epsilon_{33r}^{S''}$  from electrical measurements on a piezoelectric disk, and will be studied by the use of simulations using the TE modes model and the FE model presented in Section 2.2.3. The thickness-extensional modes model also has this limit

$$\lim_{f \rightarrow 0} \left( Y \frac{T}{i\omega A \epsilon_0} \right) = \hat{\epsilon}_{33r}^p. \quad (22)$$

Further, from the Mason TE model:

$$c_{33}^{D'} = 4\rho(f_p T)^2, \quad (23)$$

providing a method to determine  $c_{33}^{D'}$  from measurements when the TE Mason model can be used for the analyses.

### 2.2.3. FE model

The finite element program FEMP 5.0 [11, 12] is used to perform the simulations of the piezoelectric element. The direct harmonic solution method was used for simulations of the electrical admittance for the element in vacuum [12]. A simulation in vacuum compared to simulation in air introduces only a negligible error in the admittance [12], and decreases the computation time, therefore the simulations of electrical admittance are all performed in vacuum. Elements per shear wavelength was set to 5 in both radial and thickness directions for 8 nodes elements, the total number of elements is calculated at the highest simulated frequency. Furthermore, a few simulations over narrower frequency bands were made for accurate determination of resonance frequencies. The material constants used in the simulations were an adjusted set compared to the manufacturers material data. This adjusted set has been seen to give a better agreement between simulations and measurements in some earlier work [3, 13, 14]. Both the adjusted set and the set from the manufacturer are listed below. Note that the number of digits used does not indicate accuracies but are used to reduce numerical errors in calculations.

Table 1: Material data for the piezoelectric material Pz27.

Constant	Unit	Ferroperm Piezoceramics A/S	Adjusted set # 1 [13, 14]
$c_{11}^E$	[10 <sup>10</sup> Pa]	14,70	11,875(1+i $\frac{1}{95,75}$ )
$c_{12}^E$	[10 <sup>10</sup> Pa]	10,50	7,430(1+i $\frac{1}{71,24}$ )
$c_{13}^E$	[10 <sup>10</sup> Pa]	9,370	7,425 (1+i $\frac{1}{120,19}$ )
$c_{33}^E$	[10 <sup>10</sup> Pa]	11,30	11,205 (1+i $\frac{1}{177,99}$ )
$c_{44}^E$	[10 <sup>10</sup> Pa]	2,30	2,110 (1+i $\frac{1}{75}$ )
$e_{31}$	[ C · m <sup>-2</sup> ]	-3,090	-5,40 (1-i $\frac{1}{166}$ )
$e_{33}$	[ C · m <sup>-2</sup> ]	16,00	16,0389(1-i $\frac{1}{323,77}$ )
$e_{15}$	[ C · m <sup>-2</sup> ]	11,60	11,20(1-i $\frac{1}{200}$ )
$\epsilon_{11r}^S$	-	1130	916(1-i $\frac{1}{50}$ )
$\epsilon_{33r}^S$	-	914	920(1-i $\frac{1}{86,28}$ )
$\rho$	[ kg · m <sup>-3</sup> ]	7700	7700
$Q_m$	-	74	-
$\tan \delta$	-	0,017	-

In the material data from the manufacturer [15], loss is represented by the mechanical quality factor (mechanical loss)  $Q_M$  and the dielectric loss  $\tan \delta$ . In the adjusted set # 1, loss is included for all the material constants in Eqs. (12)-(14), but the values can be quite uncertain.

The simulations of the acoustical properties is made with the disk element in air. A circular layer of fluid finite elements is therefore placed outside the piezoceramic element. To ensure that the transducer radiates in to an infinite fluid, infinite elements are used outside the finite fluid elements. To reduce the computational error, the infinite elements should be placed at a distance  $R_{inf} \geq 0.32 a^2/\lambda$  [12].

### 2.3. 'Generalized permittivity'

The electrical admittance can be reformulated to the dimension of relative permittivity as [3],

$$\hat{\epsilon}_r^{GEN} \equiv \frac{YT}{i\omega\epsilon_0 A} = \frac{(G + iB)T}{i\omega\epsilon_0 A} = B \frac{T}{\omega\epsilon_0 A} - iG \frac{T}{\omega\epsilon_0 A} = \epsilon_r^{GEN'} - i\epsilon_r^{GEN''}, \quad (24)$$

where G and B are the electrical conductance and susceptance, respectively. The conductance,  $G$ , and  $\epsilon_r^{GEN''}$  are always nonnegative, and accordingly  $\epsilon_r^{GEN''}$  can also be studied in a logarithmic form, i.e  $20 \log_{10}(\epsilon_r^{GEN''})$ .

### 3. Experiment

#### 3.1. The piezoelectric disks

A set of 10 disks, of the type Pz27 [15], as illustrated in Fig. 1, with stated dimensions  $D=16$  mm and  $T=2$  mm, i.e  $D/T=8$ , were used in the present work. However, results from only one element (# 9) will be presented. The measured thickness and diameter of the element were  $T= 2.032 \pm 0.005$  mm and  $D = 16.054$  mm  $\pm 0.005$  mm giving  $D/T = 7.9006$ . The measured  $D$  and  $T$  were used together with material data for the element in FE simulations.

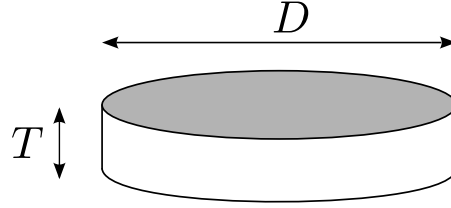


Figure 1: Illustration of a disk with diameter  $D$  and thickness  $T$ .

#### 3.2. Electrical measurements

The measurements are made using a HP 4192A impedance analyzer, as shown in Figs. 2 and 3. This impedance analyzer was connected by GPIB to a PC running MATLAB to collect the measurement data. To compensate for effects from the short wires to the element, the setup was zero-adjusted at the highest frequency for each series of measurements, according to [16].



Figure 2: Impedance analyzer HP 4192A.



Figure 3: Piezoelectric element in measurement setup.

### 4. Results

FE simulations of the electrical admittance for the element used are presented in Fig. 4 in the form of 'generalized permittivity'. The figure shows an overview of properties for the frequency range considered, 0 to 8 MHz. Separate plots will be used in the following to consider possible measuring methods for the free, the planar and the clamped permittivity constants, first by using FE to study the methods, and then using electrical measurements to apply the methods.

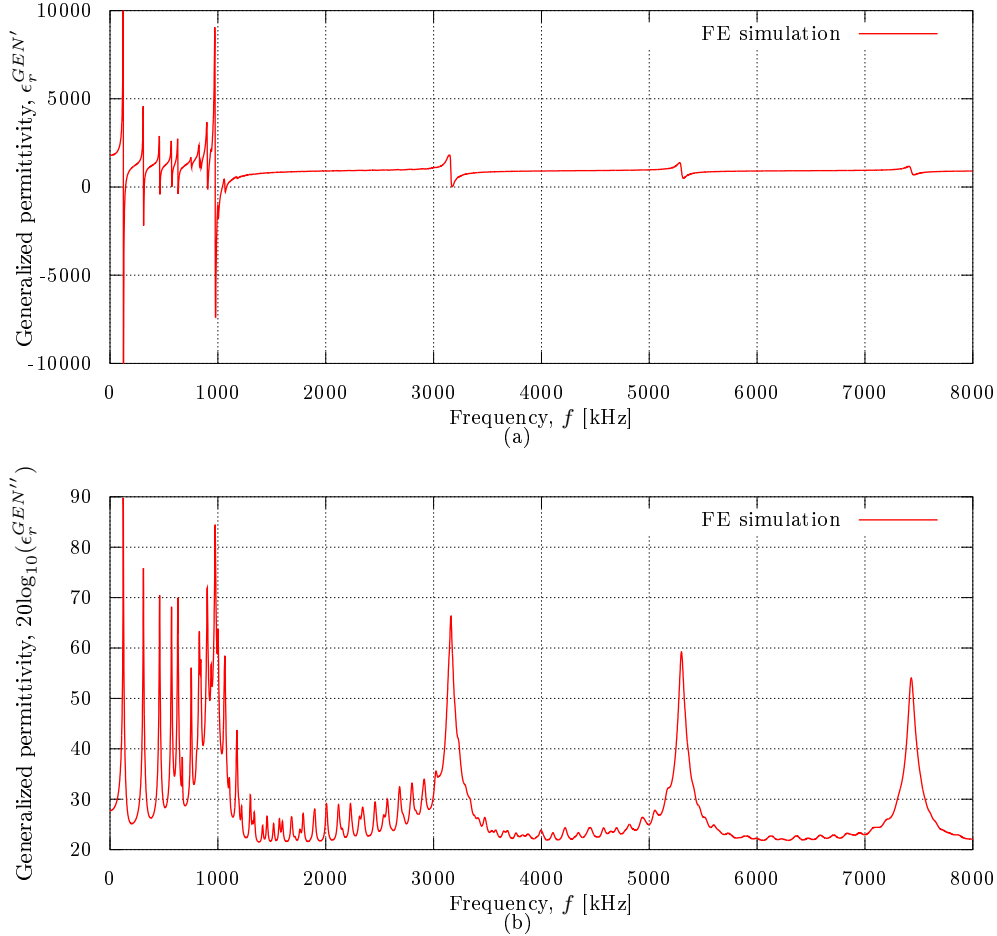


Figure 4: FE simulation of the electrical admittance reformulated as 'generalized permittivity',  $\hat{\epsilon}_r^{GEN}$ , for a Pz27 disk. (a) The real part  $\epsilon_r^{GEN'}$ , and (b) the imaginary part  $\epsilon_r^{GEN''}$ .

#### 4.1. Free permittivity constant

For the radial modes model in Section 2.2.1, the 'generalized permittivity' approaches the free permittivity constant  $\hat{\epsilon}_{33}^T$  when the frequency goes to zero. It is of interest to see if also the FE model gives this result. Also, since the permittivity of a similar piezoceramic material is known to decrease a little with frequency [17], it is of interest to see whether the free permittivity constant can be determined at a higher frequency than recommended in [4].

##### 4.1.1. Method

The IEEE Standard on Piezoelectricity 176/1987, [4], recommends to determine the free permittivity constant at a frequency lower than 1% of the first resonance frequency, i.e. the first radial mode for the disk studied, and that the  $D/T$ -ratio for the disk should be higher than 10. The method is now demonstrated with simulated data for the Pz27 element with  $D/T = 7.9$ . FE calculated 'generalized permittivity' is presented in Fig. 5 from 0.1 to 100 kHz using the adjusted set in Table 1, together with the value of  $\hat{\epsilon}_{33}^T$  calculated from this material data set.

It is seen that  $\epsilon_r^{GEN'}$  and  $\epsilon_r^{GEN''}$  both approach  $\epsilon_{33r}^{T'}$  and  $\epsilon_{33r}^{T''}$ , respectively, at low frequencies, and that even at 10 kHz, which represents 8% of the first radial resonance frequency, the deviations are less than 0.2%. This indicates that for this case with  $D/T = 7.9$ ,  $\hat{\epsilon}_{33r}^T$  can be determined with good accuracy even at 8 %

of the lowest resonance frequency. This should be an advantage considering the decrease of the permittivity constants (real parts) with frequency as seen from the measurements.

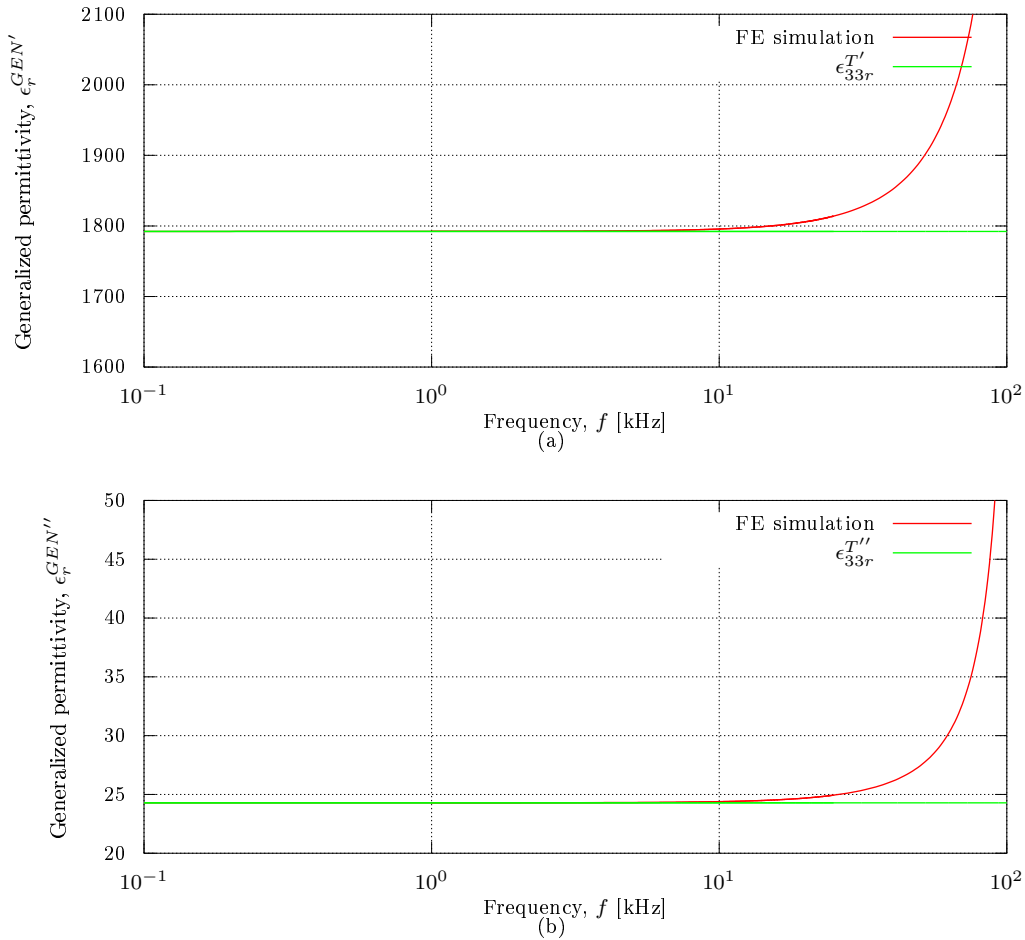


Figure 5: FE simulation of the electrical admittance reformulated as 'generalized permittivity',  $\hat{\epsilon}^{GEN}$ , for a piezoelectric disk of the material Pz27, together with the free permittivity constant,  $\hat{\epsilon}_{33r}^T$ , calculated from the adjusted set # 1 in Table 1. (a) The real parts  $\epsilon_r^{GEN'}$  and  $\epsilon_{33r}^{T'}$ , and (b) the imaginary parts  $\epsilon_r^{GEN''}$  and  $\epsilon_{33r}^{T''}$ .

#### 4.1.2. Measurements

In Fig. 6 measurements of electrical admittance reformulated as  $\epsilon_r^{GEN'}$  and  $\epsilon_r^{GEN''}$  are compared to the FE calculations and values for  $\epsilon_{33r}^{T'}$  and  $\epsilon_{33r}^{T''}$  given in Fig. 5. From the measurements  $\epsilon_{33r}^{T'}$  is seen to fall off with approximately 2.0% per decade of frequency. In [17] a similar material, PZT5A, is stated to have a decrease of 2.4% per decade for the dielectric constants to at least 20 MHz! The measurements also show that  $\epsilon_{33r}^{T''}$  increases with approximately 12.3% per decade, which for the loss factor  $\tan \delta_{33}^T$  results in an increase of 14.6% per decade. The variations with frequency have not been implemented in the FE model so far. The values of  $\epsilon_{33r}^{T'}$  and  $\epsilon_{33r}^{T''}$  from measurements at 10 kHz are:

$$\hat{\epsilon}_{33r}^T = 1766.86 - i27.97,$$

compared to the values calculated from data set # 1,

$$\hat{\epsilon}_{33r}^T = 1792.27 - i24.29.$$

The measured data, if implemented in the material constants data set, should provide a better fit for the FE simulations in this low-frequency region.

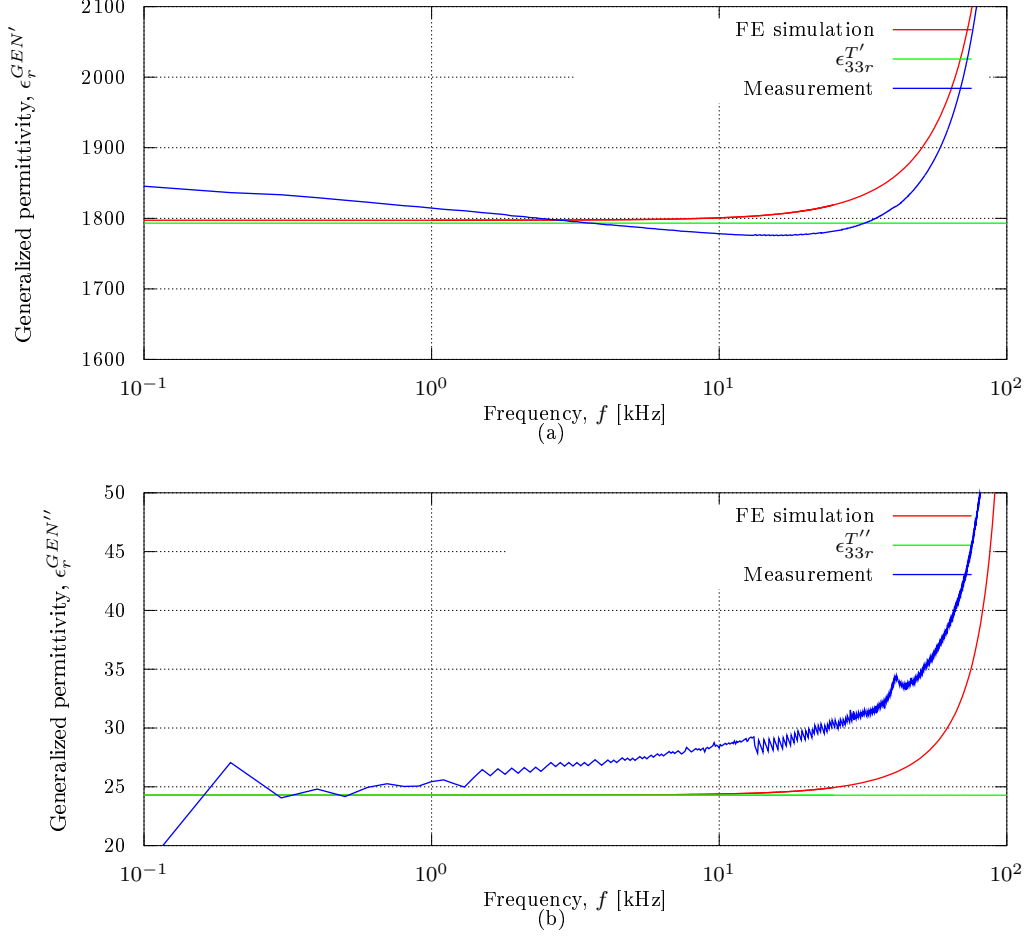


Figure 6: Measurements and FE simulation of the electrical admittance reformulated as 'generalized permittivity',  $\epsilon_r^{GEN}$ , for a Pz27 disk together with the free permittivity constant,  $\epsilon_{33r}^T$ , calculated from the adjusted set # 1 in Table 1. (a) The real parts  $\epsilon_r^{GEN'}$  and  $\epsilon_{33r}^{T'}$ , and (b) the imaginary parts  $\epsilon_r^{GEN''}$  and  $\epsilon_{33r}^{T''}$ .

#### 4.2. Planar permittivity constant

According to [4] the planar permittivity constant  $\epsilon_{33r}^{p'}$  can be determined from measured values of  $\epsilon_{33r}^{T'}$  and  $k_p'$  and the application of Eq. (5). As the simplified radial modes model gives  $\epsilon_{33r}^{p'}$  as a limiting value for  $\epsilon_r^{GEN'}$  at high frequencies, and the simplified TE modes model gives  $\epsilon_{33r}^{p'}$  as a low-frequency limit, it is of interest to see whether  $\epsilon_{33r}^{p'}$  can be determined more directly in the radial modes frequency range and before the TE modes range. FE simulations are used to study such a potential method here.

##### 4.2.1. Method

In Fig. 7 the 'generalized permittivity' is plotted for the element considered ( $D/T = 7.9$ ) using FE simulations and compared to the calculated value of  $\hat{\epsilon}_{33r}^p$  using adjusted data set # 1. In [3] similar FE studies have been done for a range of  $D/T$  from 10 to 50. For the  $\epsilon_r^{GEN'}$ , a method is used where the mean value of the maximum and minimum for each radial resonance from R2 and up to close to the edge mode region is compared with the calculated  $\hat{\epsilon}_{33r}^p$ . For all the  $D/T$  values studied in [3] and also for the present work this mean value is seen to have smallest deviation from  $\hat{\epsilon}_{33r}^p$  at R2. The method used to determine  $\epsilon_{33r}^{p''}$  from  $\epsilon_r^{GEN''}$  is to compare the minimum values between the radial modes to  $\epsilon_{33r}^{p''}$  calculated from the data set # 1 in Table 1.

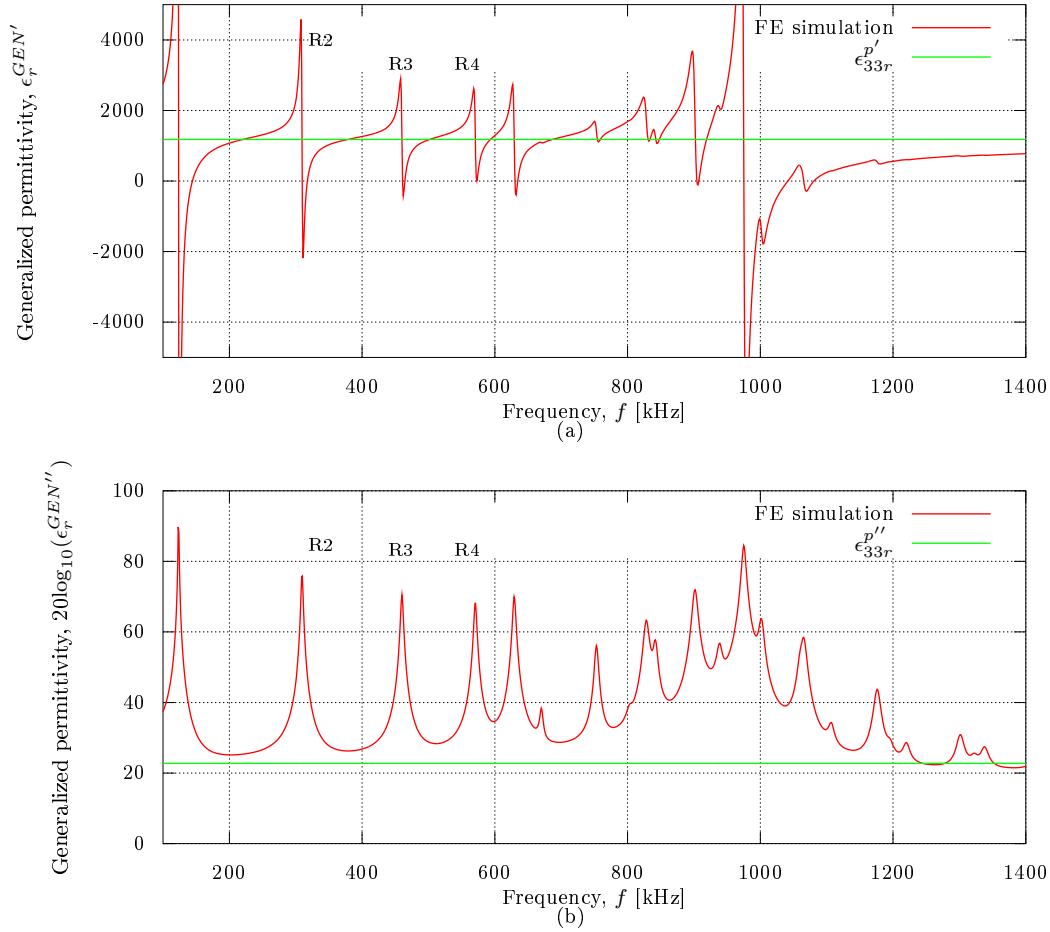


Figure 7: FE simulations of the 'generalized permittivity',  $\hat{\epsilon}_r^{GEN}$ , for a piezoelectric disk of the material Pz27, and the planar permittivity constant,  $\hat{\epsilon}_{33r}^p$ , calculated from data set # 1 in Table 1. (a) The real parts  $\epsilon_r^{GEN'}$  and  $\epsilon_{33r}^{p'}$ , and (b) the imaginary parts  $\epsilon_r^{GEN''}$  and  $\epsilon_{33r}^{p''}$ .

If these methods are used directly on the FE simulated data, the results given in Table 2 are obtained. The "Input" values are the values calculated directly from data set # 1. As can be seen the deviations between determined values and the input values increases at higher radial modes. R2 and the minimum between R1 and R2 will thus be used in the following. However, small deviations are found between the determined values and the input values, see Table 2.

Table 2: Determined  $\hat{\epsilon}_{33r}^{p'}$  and  $\hat{\epsilon}_{33r}^{p''}$  from FE simulation

	Input	R2	R3	R4
$\hat{\epsilon}_{33r}^{p'}$	1179.3	1198.5	1239.9	1311.7
$\hat{\epsilon}_{33r}^{p''}$	13,68	18.09	20.58	26.12

Such deviations are to be expected, since the R2 mode is not in a region where the  $\hat{\epsilon}_{33r}^p$  should be expected to be found exactly according to the simplified radial and TE modes models. However, the deviation is found to be fairly small both for the results in [3] and in the present results.

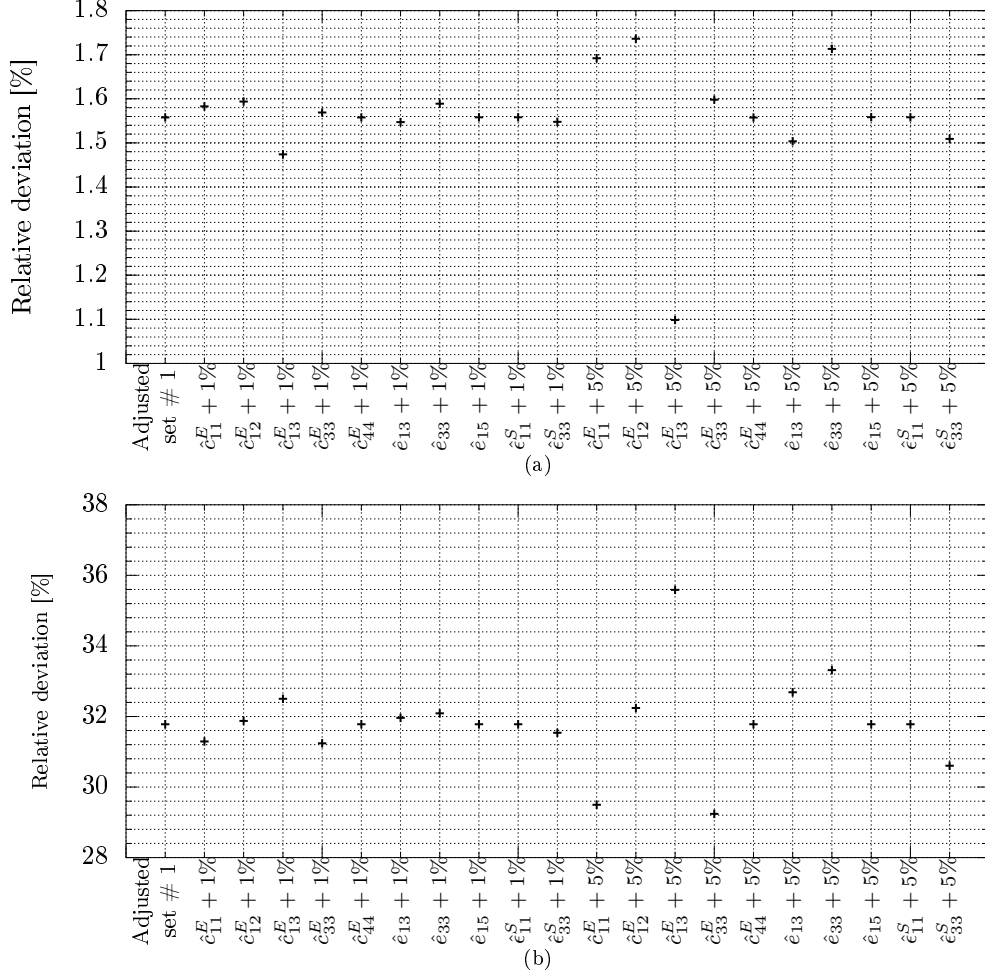


Figure 8: Sensitivity to the determination of  $\epsilon_{33r}^p$ , when the constants with loss input to the simulations are changed in value by 1% and 5%. The relative deviation is calculated through Eq.(25). (a) The relative deviation to  $\epsilon_{33r}^{p'}$ , and (b) the relative deviation to  $\epsilon_{33r}^{p''}$ .

An attempt is therefore made to compensate for these deviations when determining  $\epsilon_{33r}^p$  from measured data. One complication is that these deviations will vary to some extent with other material constants. Fig. 8 gives results from a limited sensitivity study where this deviation in % is calculated from the adjusted data set # 1 and then the material constants are varied in value one by one by 1% and 5%. The relative deviations are defined as,

$$\text{relative deviation} = \frac{\epsilon_{33r}^{p'} \text{determined} - \epsilon_{33r}^{p'} \text{calculated}}{\epsilon_{33r}^{p'} \text{calculated}} \cdot 100\%, \quad (25)$$

and similarly for  $\epsilon_{33r}^{p''}$ .

The deviations are seen to be quite insensitive to the constants  $\hat{\epsilon}_{44}^E$ ,  $\hat{\epsilon}_{15}$  and  $\hat{\epsilon}_{11}^S$ , but quite sensitive to constants such as  $\hat{\epsilon}_{11}^E$ ,  $\hat{\epsilon}_{12}^E$ ,  $\hat{\epsilon}_{13}^E$  and  $\hat{\epsilon}_{33}$ . This information may be used in an iterative method to increase the accuracy in determining  $\epsilon_{33r}^p$ . The data set # 1 results in a deviation of 1.57% for  $\epsilon_{33r}^{p'}$  and 31.6% for  $\epsilon_{33r}^{p''}$ . These values will be used in the measurement method to obtain corrected values of  $\epsilon_{33r}^p$ .

#### 4.2.2. Measurements

Measurements of the electrical admittance reformulated to the form of 'generalized permittivity' are plotted in Fig. 9 together with FE simulations and the calculated  $\epsilon_{33r}^p$  from the data set # 1 in Table 1. The

experimental values for  $\hat{\epsilon}_{33r}^p$  using the methods discussed in Section 4.2.1, are

$$\hat{\epsilon}_{33r}^p = 1040.6 - i10.056,$$

compared to FE simulations data which give:

$$\hat{\epsilon}_{33r}^p = 1179,3 - i13.68,$$

using data set # 1. However, in particular the experimental value for  $\epsilon_{33r}^{p''}$  is considered to be quite inaccurate. As can be seen from Fig. 9 the variation of the measured  $\epsilon_r^{GEN''}$  between R1 and R2 deviates significantly in shape from the FE calculations. The data set # 1 is thus seen not to recreate this measured variation very well, which results in problems in determining a representative minimum between the two radial resonance frequencies. Future improved methods to determine the material constants in Table 1 in addition to possible iterations are expected to provide a more accurate determination of  $\epsilon_{33r}^{p''}$ .

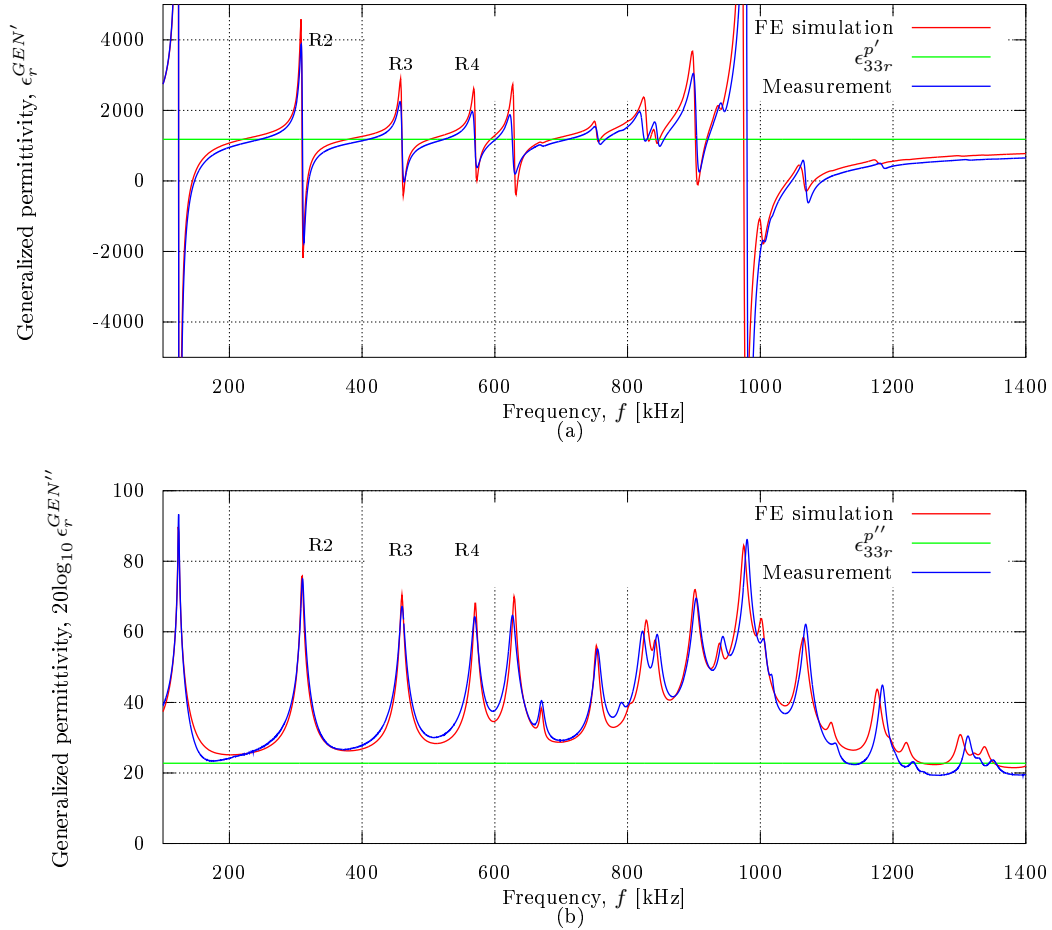


Figure 9: Measurements together with FE simulations of the 'generalized permittivity',  $\hat{\epsilon}_r^{GEN}$ , for a piezoelectric disk of the material Pz27, and the planar permittivity constant,  $\hat{\epsilon}_{33r}^p$ , calculated from data set # 1 in Table 1.(a) The real parts  $\epsilon_r^{GEN'}$  and  $\epsilon_{33r}^p$ , and (b) the imaginary parts  $\epsilon_r^{GEN''}$  and  $\epsilon_{33r}^{p''}$ .

### 4.3. Clamped permittivity constant

In Section 2.2.2 and Eq. (19) a method based on the MasonTE model for determining  $\epsilon_{33r}^S$  is discussed. Early unpublished work by Magne Aanes showed, using FE modeling, that the method provided quite accurate results for a piezoceramic disk. This method is investigated further in Section 4.3.1 and applied on measured electrical admittance and impedance data in Section 4.3.2. Note that the IEEE Standard on Piezoelectricity,

[4], does not recommend to determine the clamped permittivity constant at high frequencies because the presence of unwanted modes will make it difficult to obtain reliable data.

#### 4.3.1. Method

The 'generalized permittivity' based on FE simulations using data set # 1 is shown in Fig. 10 over a frequency range that covers the first four TE resonances. Results for the Mason TE model is plotted for comparisons together with lines for  $\hat{\epsilon}_{33}^S$  taken from the data in Table 1. In Table 3 the four parallel resonance frequencies for these TE resonances are given for both the FE simulations and the Mason TE model together with the midpoint frequencies according to the two models.

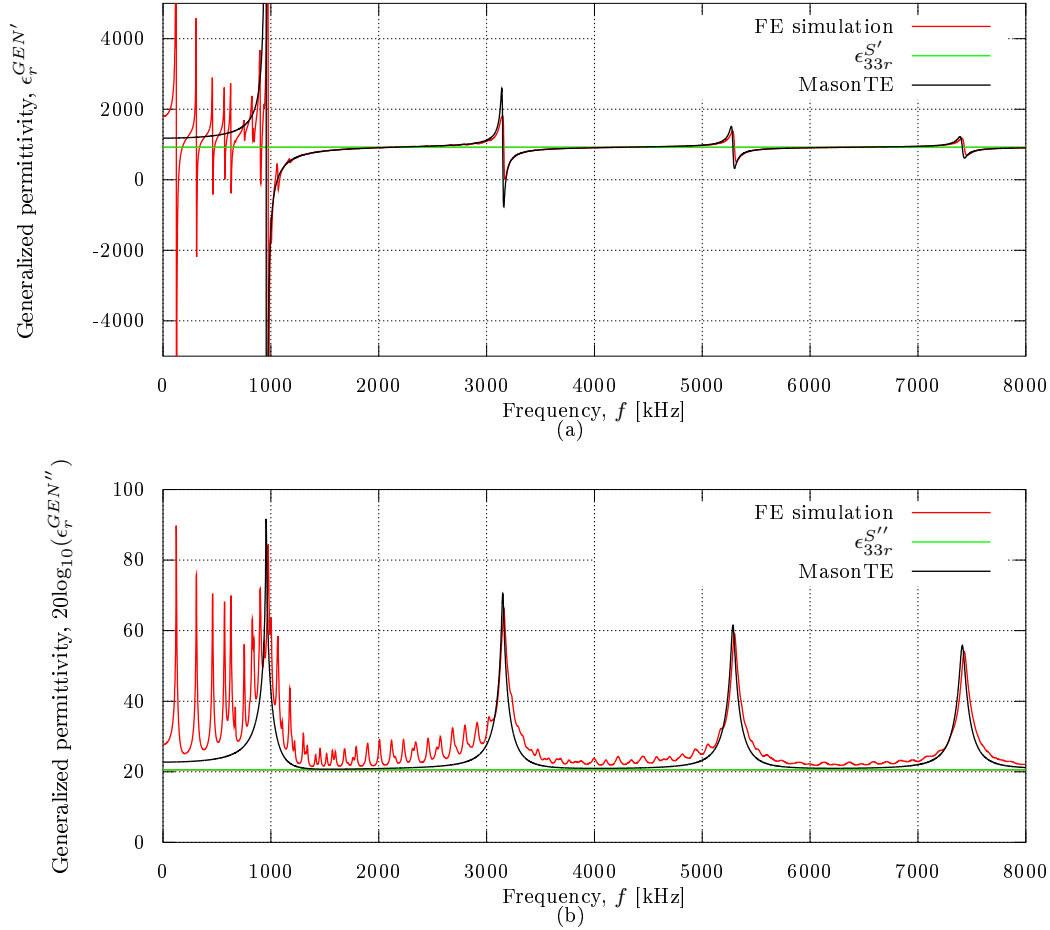


Figure 10: The 'generalized permittivity',  $\epsilon_r^{GEN}$ , for a piezoelectric disk of material Pz27, from FE and Mason TE model simulations using data set # 1 in Table 1, together with  $\hat{\epsilon}_{33}^S$  from the same data set. (a) The real parts  $\epsilon_r^{GEN'}$  and  $\epsilon_{33r}^{S'}$ , and (b) the imaginary parts  $\epsilon_r^{GEN''}$  and  $\epsilon_{33r}^{S''}$ .

Table 3: Parallel resonance frequencies and midpoint frequencies for determining the  $\hat{\epsilon}_{33}^S$  based on using FE simulations with data from data set # 1 in Table 1 and also compared with using the Mason TE model for the same data set.

	$f_{p1}$ [MHz]	$f_{p2}$ [MHz]	$f_{p3}$ [MHz]	$f_{p4}$ [MHz]	$\frac{f_{p1}+f_{p2}}{2}$ [MHz]	$\frac{f_{p2}+f_{p3}}{2}$ [MHz]	$\frac{f_{p3}+f_{p4}}{2}$ [MHz]
MasonTE	1.0631	3.1884	5.3147	7.4399	2.1253	4.2515	6.3768
FE simulation	1.081	3.188	5.316	7.442	2.1345	4.252	6.379

The method to determine  $\hat{\epsilon}_{33r}^S$  described in Section 2.2.2 can thus be tested using simulated data instead of measurements. The results from this test is given in Table 4 for the different midpoint frequencies. These results can be compared to the input data for  $\hat{\epsilon}_{33r}^S$  given in Table 1, and should be expected to give a close fit if the method is good. This fit should be expected to be particularly close for the Mason model, which is also seen to be the case especially for  $\epsilon_{33r}^{S'}$ . The agreement is also reasonably good for the FE simulations data, but with some deviations and in particular for  $\epsilon_{33r}^{S''}$ . The deviations seen may in part be due to complications from the spurious resonances seen between the TE modes. To illustrate these effects expanded plots are given in Fig. 11 around the midpoint frequencies where  $\hat{\epsilon}_{33r}^S$  is determined. Even with the small deviations noticed, the results are seen to be promising, in particular for  $\epsilon_{33r}^{S'}$ .

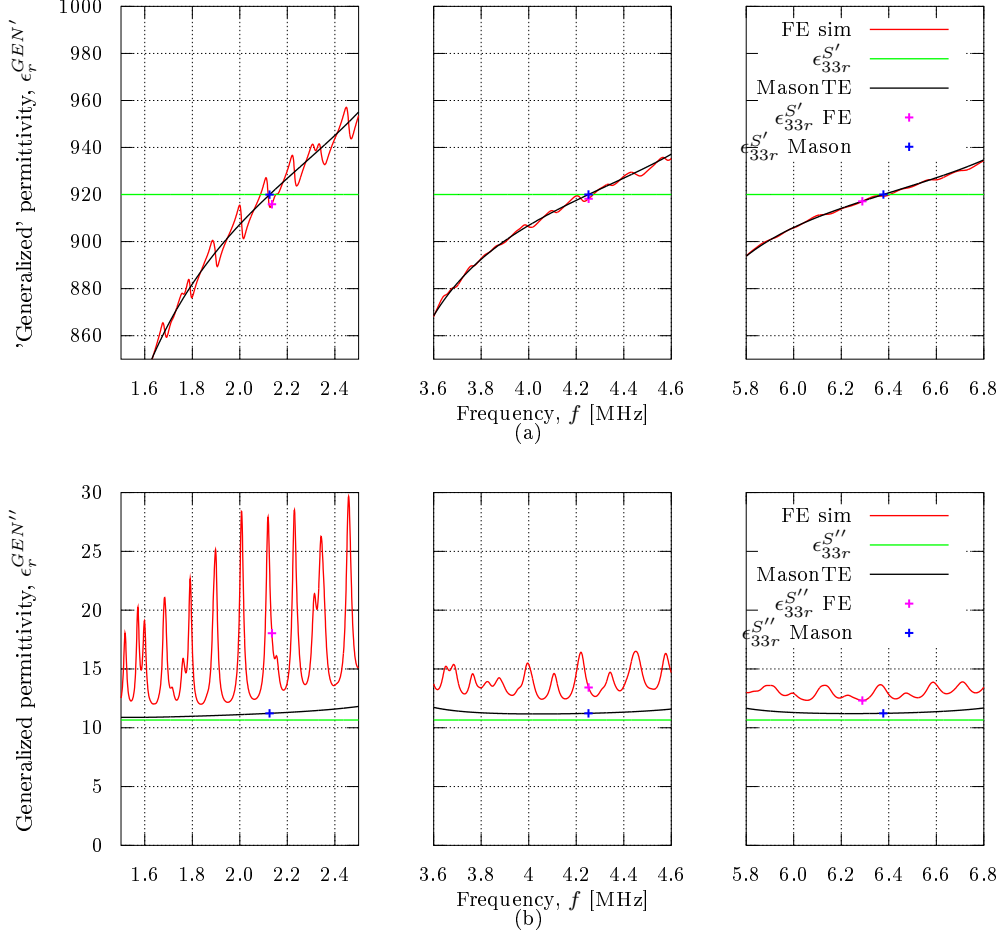


Figure 11: Expanded views of the simulated 'generalized permittivity',  $\hat{\epsilon}_r^{GEN}$ , shown in Fig. 10 and the clamped permittivity constant,  $\hat{\epsilon}_{33r}^S$ , from data set # 1, at frequency regions where  $\hat{\epsilon}_{33r}^S$  is determined. (a) The real parts  $\epsilon_r^{GEN'}$  and  $\epsilon_{33r}^{S'}$ , and (b) the imaginary parts  $\epsilon_r^{GEN''}$  and  $\epsilon_{33r}^{S''}$ .

Table 4:  $\hat{\epsilon}_{33r}^S$  determined from simulated  $\hat{\epsilon}_r^{GEN}$  using FE simulations and also the Mason TE model.

Between parallel resonances	$\epsilon_{33r}^{S'}$ from Mason	$\epsilon_{33r}^{S''}$ from Mason	$\epsilon_{33r}^{S'}$ from FE simulation	$\epsilon_{33r}^{S''}$ from FE simulation
1-2	919.96	11.23	915.67	18.385
2-3	920.00	11.23	918.22	13.427
3-4	919.99	11.23	917.10	12.314

### 4.3.2. Measurements

To use the method described in Section 4.3.1 on measured data, the measured electrical admittance recalculated as 'generalized permittivity' is plotted in Fig. 12 together with the same simulated curves as in Fig. 10 for comparisons. Noticeable differences are seen here between the measurements and simulations demonstrating that the data set # 1 in Table 1 does not give a very close fit for this piezoelectric element.

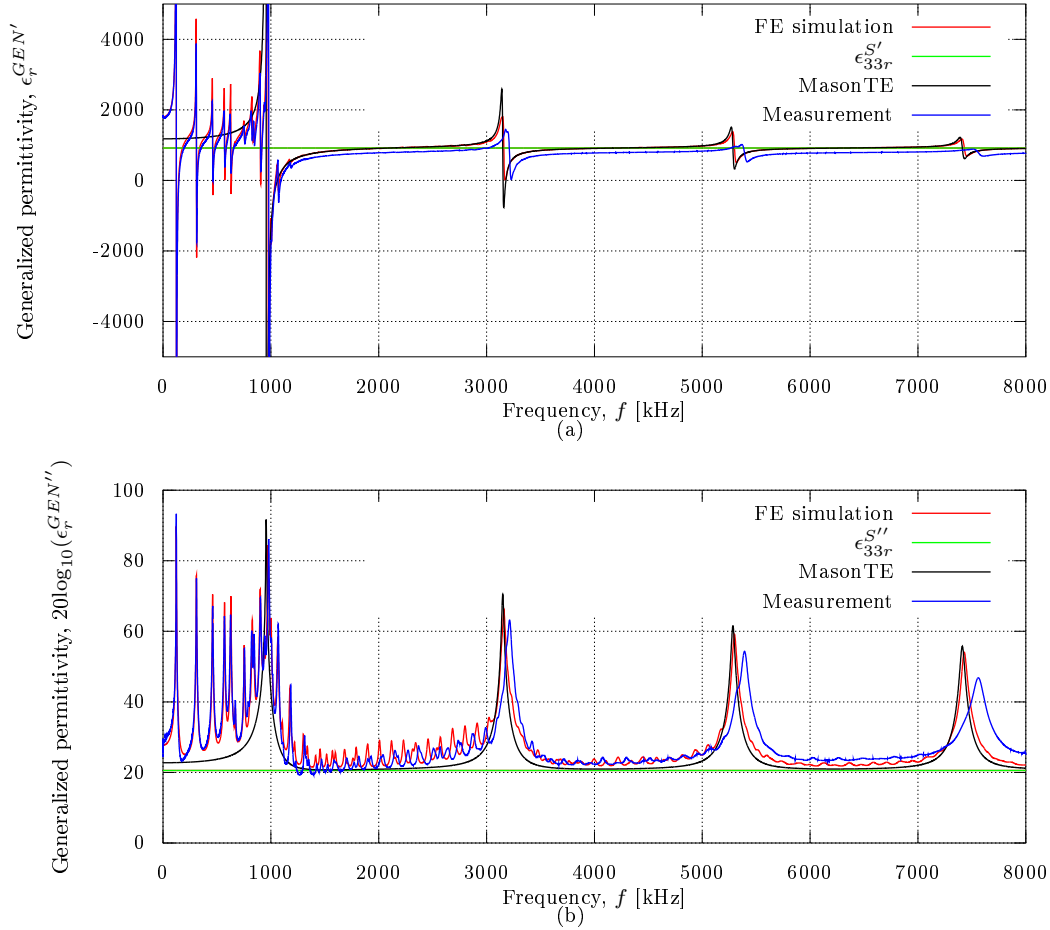


Figure 12: Measurements together with FE and Mason TE model simulations of 'generalized permittivity',  $\hat{\epsilon}_r^{GEN}$ , for a piezoelectric disk of material Pz27 using data set # 1 in Table 1, and  $\hat{\epsilon}_{33r}^S$  from the same data set. (a) The real parts  $\epsilon_r^{GEN'}$  and  $\epsilon_{33r}^{S'}$ , and (b) the imaginary parts  $\epsilon_r^{GEN''}$  and  $\epsilon_{33r}^{S''}$ .

In Table 5 the parallel resonance frequencies for the four TE modes are given together with the three midpoint frequencies where the values for  $\hat{\epsilon}_{33r}^S$  are taken. Expanded views of the measured results for  $\hat{\epsilon}_r^{GEN}$  are shown in Fig. 13 around the three midpoint frequencies, and illustrates how the spurious resonances affect the determination of  $\hat{\epsilon}_{33r}^S$ .

Table 5: Parallel resonances and midpoint frequencies for measurements on a Pz27 disk

	$f_{p1}$	$f_{p2}$	$f_{p3}$	$f_{p4}$	$\frac{f_{p1}+f_{p2}}{2}$	$\frac{f_{p2}+f_{p3}}{2}$	$\frac{f_{p3}+f_{p4}}{2}$
	[MHz]	[MHz]	[MHz]	[MHz]	[MHz]	[MHz]	[MHz]
Measurements	1.0942	3.2429	5.411	7.573	2.1686	4.3270	6.4920

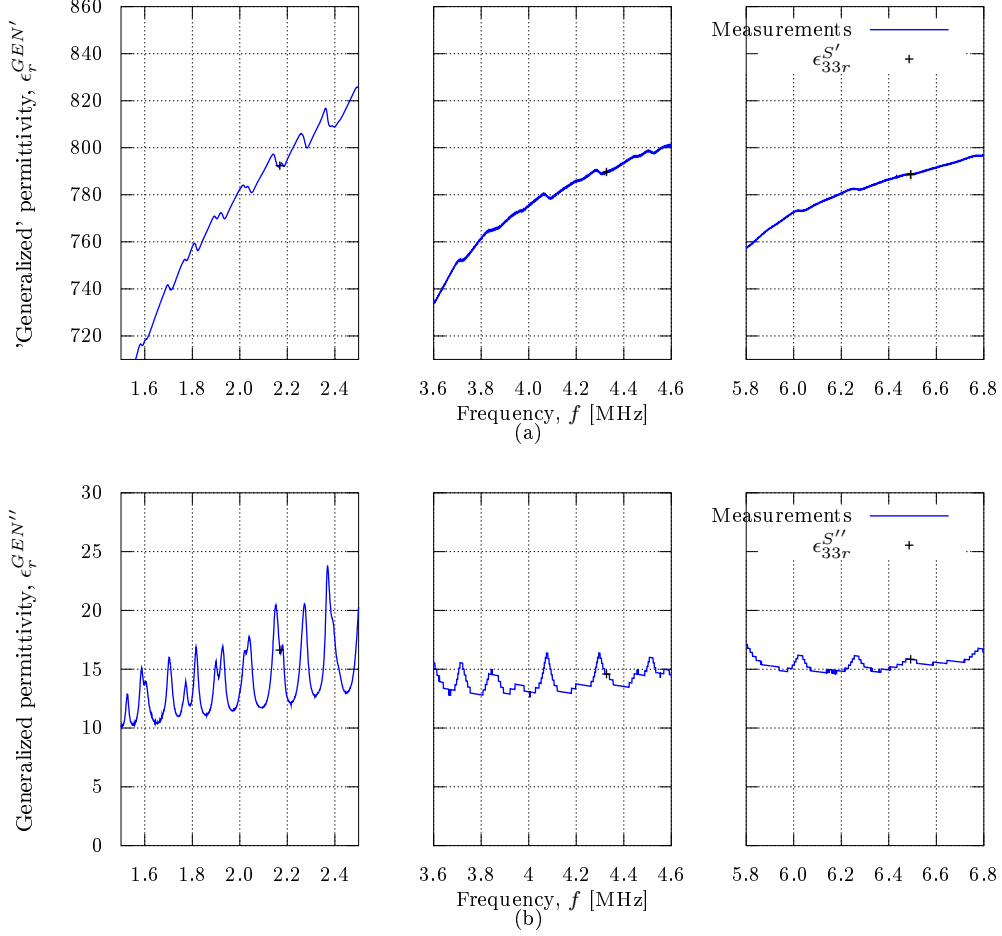


Figure 13: Expanded views of the measured 'generalized permittivity',  $\epsilon_r^{GEN}$ , shown in Fig. 12, at frequency regions where  $\epsilon_{33r}^S$  is determined. (a) The real part  $\epsilon_r^{GEN'}$ , and (b) the imaginary part  $\epsilon_r^{GEN''}$ . Points where the permittivity constants are determined, are indicated by + (uncorrected).

Table 6:  $\hat{\epsilon}_{33r}^S$  determined from measurements, calculated  $\tan \delta_{33}^S$  and  $Q_{33}^S$

Between parallel resonances	$\epsilon_{33r}^{S'}$ from measurements	$\epsilon_{33r}^{S''}$ from measurements	$\tan \delta_{33}^S$	$Q_{33}^S$
1-2	792.38	16.636	0.021	47.63
2-3	789.86	14.549	0.018	54.29
3-4	787.86	15.841	0.020	49.74

Results for  $\hat{\epsilon}_{33r}^S$  are given in Table 6 including values for  $\tan \delta_{33}^S$  and  $Q_{33}^S$ . As illustrated for the simulated data in Section 4.3.1, the method is also assumed to be best at the highest of the midpoint frequencies for the measurements. By using in addition a correction of +0.32% for  $\epsilon_{33r}^{S'}$  and -15.52% for  $\epsilon_{33r}^{S''}$ , as obtained by using the FE simulations as described in Section 4.3.1, the following values are obtained,

$$\hat{\epsilon}_{33r}^S = 790.38 - i13.713.$$

The values from Table 1 are, for comparisons:

$$\hat{\epsilon}_{33r}^S = 920.00 - i10.66.$$

These measured values are thus seen to deviate significantly from the values from Table 1. This can also be readily seen from the plots of measurements and FE simulations in Fig. 12. The values for  $\hat{\epsilon}_{33r}^S$  in Table 1 are therefore clearly wrong for the piezoceramic element studied.

#### 4.4. Additional constants and a new adjusted set of material data

By using the Mason TE model for analysis, the stiffness constant  $c_{33}^{D'}$  can be determined from measurements as shown in Section 2.2.2 Eq. (23). To test, by using FE simulations, whether this can provide an accurate method for an element such as the one considered here, values for  $c_{33}^{D'}$  are given in Table 7 both by using simulations (Mason TE model and FE model) and from measurements. The parallel resonance frequencies for the four TE resonances are used as indicated in the table, and for the simulations the results for  $c_{33}^{D'}$  should be compared with the calculated value from data set # 1 in Table 1;  $c_{33}^{D'} = 14.363 [10^{10} \text{ Pa}]$ . The Mason model gives as expected very close agreement, but what is important here is that also the FE simulated data give very close agreement for the two highest parallel resonance frequencies, and for the highest the deviation is +0.059%. Thus it is expected that  $c_{33}^{D'}$ , when it is corrected by -0.059% is determined fairly accurately to the value,

$$c_{33}^{D'} = 14.873 [10^{10} \text{ Pa}]$$

For the corresponding loss constant no new measurement has been done here, and the value calculated from material data set # 1 in Table 1 will be used.

Table 7: Determination of  $c_{33}^{D'}$  from simulations and measurements using Eq.(23).

Unit	$c_{33}^{D'}$ [10 <sup>10</sup> Pa]	$c_{33}^{D'}$ [10 <sup>10</sup> Pa]	$c_{33}^{D'}$ [10 <sup>10</sup> Pa]	$c_{33}^{D'}$ [10 <sup>10</sup> Pa]
Using frequency	$f_{p1}$	$f_{p2}/3$	$f_{p3}/5$	$f_{p4}/7$
MasonTE	14.370	14.362	14.366	14.363
FE simulation	14.858	14.358	14.373	14.371
Measurements	15.223	14.857	14.891	14.882

By using Eq. (11) the constants  $\hat{c}_{33}^E$  and  $\hat{\epsilon}_{33}$  can now be determined using the results given above. For the constants in Table 1 that are redetermined in the present work, i.e  $\hat{c}_{33}^E$ ,  $\hat{\epsilon}_{33}$  and  $\hat{\epsilon}_{33r}^S$ , the values are used together with constants from data set # 1 in Table 1 to give a new adjusted material constants data set # 2 as shown in Table 8.

Table 8: Material data for the piezoelectric material Pz27.

Constant	Unit	Ferroperm Piezoceramics A/S	Adjusted set # 1[13, 14]	Adjusted set # 2
$c_{11}^E$	[10 <sup>10</sup> Pa]	14,70	11,875(1+i $\frac{1}{95,75}$ )	11,875(1+i $\frac{1}{95,75}$ )
$c_{12}^E$	[10 <sup>10</sup> Pa]	10,50	7,430(1+i $\frac{1}{71,24}$ )	7,430(1+i $\frac{1}{71,24}$ )
$c_{13}^E$	[10 <sup>10</sup> Pa]	9,370	7,425 (1+i $\frac{1}{120,19}$ )	7,425 (1+i $\frac{1}{120,19}$ )
$c_{33}^E$	[10 <sup>10</sup> Pa]	11,30	11,205 (1+i $\frac{1}{177,99}$ )	11,298(1+i $\frac{1}{439,29}$ )
$c_{44}^E$	[10 <sup>10</sup> Pa]	2,30	2,110 (1+i $\frac{1}{75}$ )	2,110 (1+i $\frac{1}{75}$ )
$e_{31}$	[ C · m <sup>-2</sup> ]	-3,090	-5,40 (1-i $\frac{1}{166}$ )	-5,40 (1-i $\frac{1}{166}$ )
$e_{33}$	[ C · m <sup>-2</sup> ]	16,00	16,0389(1-i $\frac{1}{323,77}$ )	15,8216(1-i $\frac{1}{162,10}$ )
$e_{15}$	[ C · m <sup>-2</sup> ]	11,60	11,20(1-i $\frac{1}{200}$ )	11,20(1-i $\frac{1}{200}$ )
$\epsilon_{11r}^S$	-	1130	916(1-i $\frac{1}{50}$ )	916(1-i $\frac{1}{50}$ )
$\epsilon_{33r}^S$	-	914	920(1-i $\frac{1}{86,28}$ )	790,38(1-i $\frac{1}{57,63}$ )
$\rho$	[ kg · m <sup>-3</sup> ]	7700	7700	7700
$Q_m$	-	74	-	-
$\tan \delta$	-	0,017	-	-

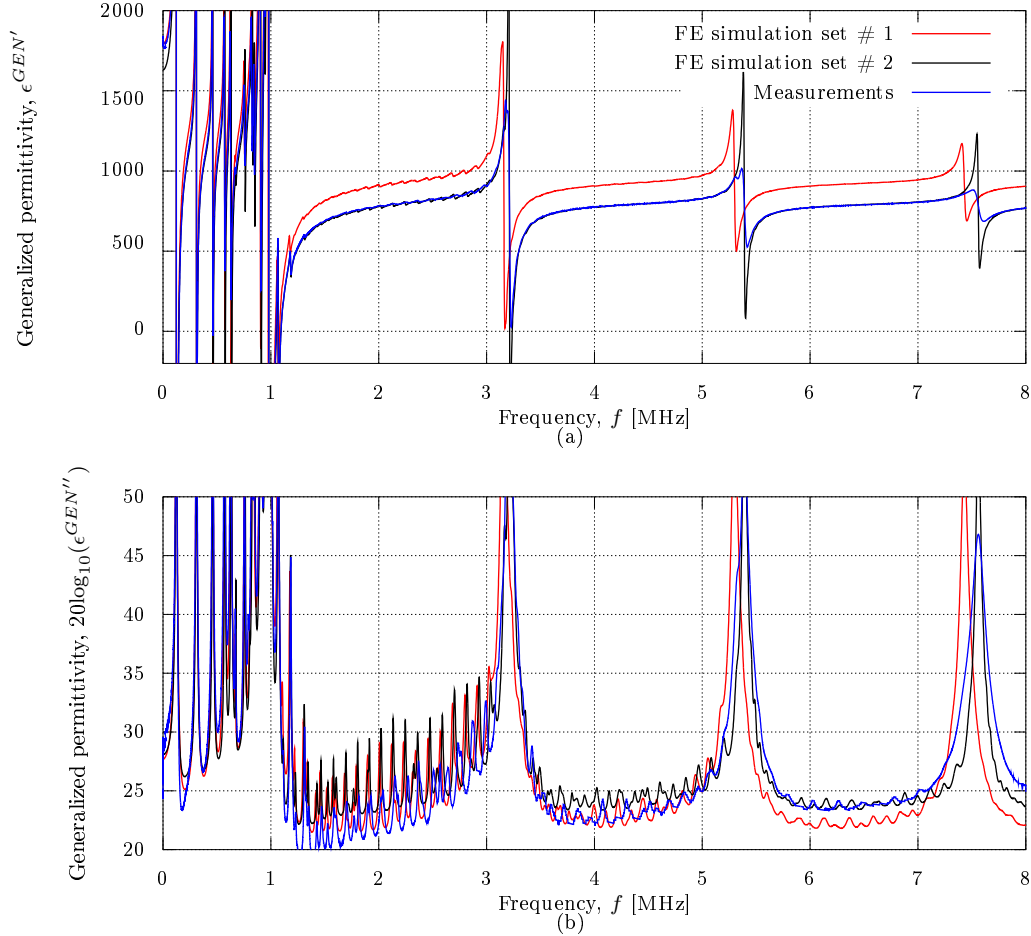


Figure 14: FE simulation of the 'generalized' permittivity,  $\epsilon_r^{GEN}$ , for a Pz27 disk using two different set of material data, set # 1 and set # 2, together with measurements. (a) The real part, and (b) the imaginary part.

In Fig. 14 the new data set # 2 is used to obtain a new FE simulation for the 'generalized permittivity' of the element, which should be expected to give a closer fit in particular in the high frequency region and for the parts of the curves where the determined constants should be expected to have an effect. This is also seen to be the case. On the other hand, further adjustments are seen to be needed for the remaining constants in Table 8. In the low-frequency region the measurements of  $\epsilon_{33r}^T$  have not been utilized in the adjustments in data set # 2 so far. Further, for the lower part of the radial modes region it is also well known through FE sensitivity analyses [2, 18] that the three constants  $c_{44}^E$ ,  $e_{15}$  and  $\epsilon_{11}^S$  have little effect on the electrical properties. Such information can be important in the work to develop improved measurement methods for the additional constants in Table 8.

#### 4.5. Source sensitivity

The effects of the adjustments in material constants data from data set # 1 to data set # 2 in Table 8 on the FE calculated source sensitivity is shown in Fig. 15 from 0 to 200 kHz. The results show a small shift in frequency of the resonance peak and an approximately 2.7 dB higher source sensitivity at the peak than by using data set # 1. This is a noticeably large change in sensitivity. It will be important to look more into the effects of the various constants on the electro-acoustical and acoustical properties generated by such a piezoceramic element, in order to evaluate how accurately acoustical properties can be determined by FE simulations from a given set of material constants data.

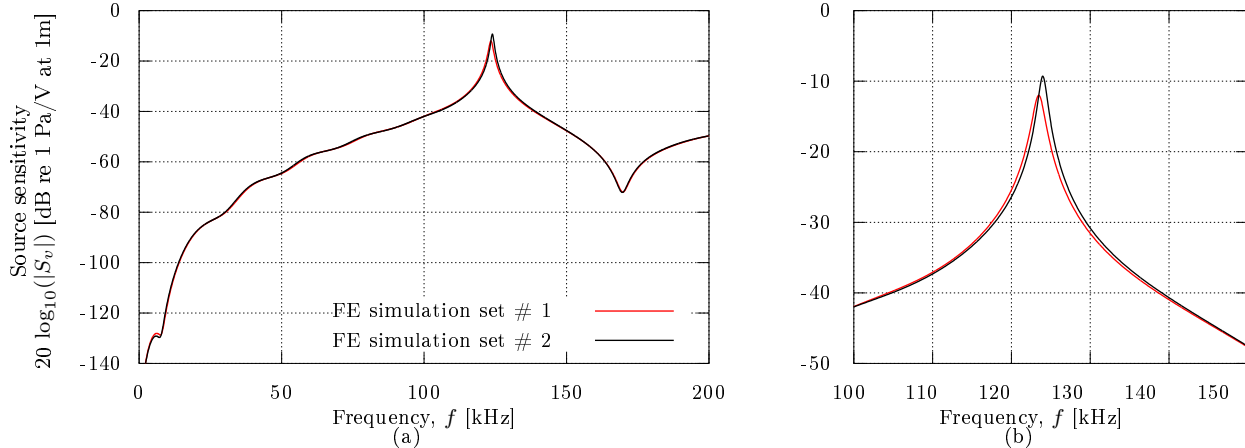


Figure 15: Simulated source sensitivity for a Pz27 disk radiating in air using two different material data sets, set # 1 and set # 2 in Table 8. All other simulation parameters are kept identical. (a) 0 – 200 kHz frequency range (b) expanded plot in the region of the R1 resonance peak.

## 5. Conclusions

The 'generalized permittivity' formulation of the electrical admittance of a piezoceramic disk is used through FE simulations to study methods for determining the free ( $\hat{\epsilon}_{33}^T$ ), the planar ( $\hat{\epsilon}_{33}^P$ ) and the clamped ( $\hat{\epsilon}_{33}^S$ ) permittivity constants. In addition, a method for determining the stiffness constant at constant electrical displacement is studied using FE simulations. Use of the methods on electrical measurements provide data for these and two other material constants which together are used to derive a new adjusted material constants data set for the piezoceramic element studied. The effects of the changes in material constants data on the FE simulated source sensitivity are also studied. Further experience on other piezoceramic disk elements of other materials and sizes are needed both to confirm the physical soundness of the methods, to study the measurement uncertainty which can be achieved, and also to study the effects of different material constants on electro-acoustical and acoustical properties. Further work is also needed to develop physically sound improved methods for determining the remaining material constants.

## Acknowledgement

PhD candidate Espen Storheim is greatly acknowledged for useful discussions and general help in the lab throughout the preparation of this paper.

## References

- [1] T. Lahmer, M. Kaltenbacher, B. Kaltenbacher, R. Lerch, and E. Leder, "FEM-Based determination of real and complex elastic, dielectric, and piezoelectric moduli in piezoceramic materials", *IEEE Trans. Ultrason. Ferroelectr. Freq. Control* **55**(2), 465–475 (2008).
- [2] N. Pe Andrez, M. Andrade, F. Buiochi, and J. Adamowski, "Identification of elastic, dielectric, and piezoelectric constants in piezoceramic disks", *IEEE Trans. Ultrason. Ferroelectr. Freq. Control* **57**(12), 2772–2783 (2010).
- [3] M. Aanes, "Undersøkelser av piezokeramiske skiver. Målinger og endelig element analyser.", Master thesis, Dept. of Physics and Technology, University of Bergen, Bergen, Norway (2009), (in Norwegian).
- [4] ANSI/IEEE, "IEEE Standard on Piezoelectricity - ANSI/IEEE Std. 176", (1987).

- [5] International Electromechanical Commission, “Guide to dynamic measurements of piezoelectric ceramics with high electromechanical coupling”, IEC Publication 483 (1976).
- [6] P. Lunde and M. Vestrheim, “Piezoelectric transducer modeling part 1: Basic equations for poled ferroelectric ceramics”, CMI report no.: CMI-91-A10010, Chr. Michelsen Institute, Bergen, Norway (December, 1991).
- [7] R. Holland, “Representation of dielectric, elastic, and piezoelectric losses by complex coefficients”, IEEE Trans. Sonics and Ultrasonics **14**(1), 18 – 20 (1967).
- [8] M. Vestrheim, “PHYS 373 - Akustiske Målesystemer”, Lecture notes, Dept. of Physics and Technology, University of Bergen, Bergen, Norway (2008), (in Norwegian).
- [9] A. Meitzler, J. O’Byryan, H.M., and H. Tiersten, “Definition and Measurement of Radial Mode Coupling Factors in Piezoelectric Ceramic Materials with Large Variations in Poisson’s Ratio”, IEEE Trans. Sonics and Ultrasonics **20**(3), 233 – 239 (1973).
- [10] G.Lypacewicz and L.Filipczyński, “Measurements of the Clamped Capacitance  $C_0$  and the Electromechanical Coupling Coefficient  $k_t$  of Ceramic Transducers under Mechanical Load”, Acustica **25**(1), 64 – 68 (1971).
- [11] J. Kocbach, P. Lunde, M. Vestrheim, R. Kippersund, “Finite element modeling of ultrasonic piezoelectric transducers. Extension of FEMP to 3D analysis”, CMR report no.: CMR-06-A10046-RA-01, Christian Michelsen Research AS, Bergen, Norway (December 2006).
- [12] J. Kocbach, “Finite Element Modeling of Ultrasonic Piezoelectric Transducers”, PhD thesis, Dept. of Physics and Technology, University of Bergen, Bergen, Norway (2000).
- [13] K. D. Lohne, “Undersøkelse og Utnyttelse av Svingemoder i Ultralyd Transduserkonstruksjoner.”, Master thesis, Dept. of Physics and Technology, University of Bergen, Bergen, Norway (2005), (in Norwegian).
- [14] V. Knappskog, “Radiellmode svingninger i piezoelektriske ultralydtransdusere for luft. Målinger og endelig element analyser”, Master thesis, Dept. of Physics and Technology, University of Bergen, Bergen, Norway (2007), (in Norwegian).
- [15] Ferroperm Piezoceramics A/S, now a member of Meggitt’s Sensing Systems division, “High quality components and materials for the electronic industry”, DK-3490 Kvistgård (2003).
- [16] Hewlett Packard, *Operation and Service Manual: 4192 LF Impedance Analyzer* (1981).
- [17] Vernitron, “Five Modern Piezoelectric Ceramics”, Vernitron Ltd. England (now Morgan Technical Ceramics) (1987).
- [18] R. Fardal, “Endelig Element Analyse av Elektriske Egenskaper til Piezoelektriske Skiver”, Master thesis, Dept. of Physics and Technology, University of Bergen, Bergen, Norway (2002), (in Norwegian).